Electronic structure calculations and dynamics of methane activation on nickel and cobalt

Electronic structure calculations and dynamics of methane activation on nickel and cobalt

H. Burghgraef, A. P. J. Jansen, and R. A. van Santen
Laboratory for Inorganic Chemistry and Catalysis/Theory Group, Eindhoven University of Technology, P.O. Box 513, 5600 MB Eindhoven, The Netherlands

(Received 29 June 1994; accepted 29 August 1994)

The dissociative chemisorption of CH_4 on nickel and cobalt has been studied using different cluster models. Density functional theory is used to determine the structure and potential energy surface in the reactant-, transition state-, and product region. The transition state is explicitly determined on a single atom, a one layer 7-atom cluster and a spherical 13-atom cluster. We find transition state barriers of 41 kJ/mol for a single nickel atom, 79 kJ/mol for a single cobalt atom, 214 kJ/mol for the Ni_7-cluster, 216 kJ/mol for the Co_7-cluster, 121 kJ/mol for the Ni_{13}-cluster, and 110 kJ/mol for the Co_{13}-cluster. The overall reaction energies are −34, 6, 142, 135, 30, and 8 kJ/mol, respectively. The higher barrier for the single cobalt atom in comparison with the nickel atom can be attributed to the difference between both atoms in the occupation of the *s*-orbital in the lowest lying states. The higher and almost the same barrier for the 7-atom clusters can be attributed to the intrinsic lower reactivity of the central atom embedded in the cluster and the similar electronic nature of the atoms in the clusters; in both clusters the atoms have open *s*- and *d*-shells. The lower barrier for the 13-atom clusters compared with the 7-atom clusters is a result of each surface atom now having 5 bonds, which gives a more balanced description of the substrate model.

I. INTRODUCTION

Two very interesting and important reactions in heterogeneous catalysis are the steam reforming of methane to produce hydrogen[1] and the Fischer–Tropsch synthesis, where carbon monoxide and hydrogen produce methane among higher hydrocarbons.[2] In the first reaction, the rate determining step is the dissociative chemisorption of CH_4 and industrially interesting conversion levels can only be achieved at high temperatures and pressures and in the presence of a transition metal catalyst.[3] The difficult decomposition of CH_4 is attributed to the barrier for breaking the CH bond. This reaction has been studied experimentally and theoretically by various groups and we have discussed the results extensively in previous papers.[4] In the second reaction, it was concluded by Yates *et al.*[5] that the rate determining step to form CH_4 occurred in an earlier stage than the recombination of adsorbed methyl and hydrogen. Whether CH_4 or higher hydrocarbons are produced depends strongly on the metal catalyst and on reaction conditions, but over metals like Fe, Co, and Ru a wide range of hydrocarbons is formed, whereas over Ni and Pd methane is the principle product, while Cu shows no reactions at all.[6]

Previous computational studies on CH_4 dissociation focused mainly on electronic structure calculations[7] or on treating the dynamics using a model for the potential energy surface. Luntz *et al.*[8] argue that the dissociation mechanism is dominated by quantum mechanical tunneling involving a potential energy surface of at least three degrees of freedom, suggesting that a classical approach to CH_4 dissociation is not appropriate. However, we feel that under the condition of rapid energy exchange compared to the overall reaction time, which is valid in the case of a high activation barrier and at high temperatures and pressures, which are the industrial conditions of CH_4 steam reforming, transition state theory may be applicable. Also in the case of a wide activation barrier, the importance of tunneling will decrease. Therefore, we have calculated both the potential energy surface at the reactant region, transition state, and product region using an *ab initio* density functional approach, and treated the kinetics of the system by employing transition state theory. Specifically, we have taken a single atom, a one layer 7-atom cluster, and a 13-atom cluster to model the substrate. Thus we have for the single atom model a bimolecular insertion reaction and a unimolecular elimination reaction,

$$CH_4 + M \xrightarrow{k_{\text{bi.ins.}}} HMCH_3, \tag{1}$$

and

$$HMCH_3 \xrightarrow{k_{\text{uni.eli.}}} CH_4 + M, \tag{2}$$

and for the 7- and 13-atom clusters a dissociative adsorption of CH_4 and an associative desorption of CH_3 and H,

$$CH_4 + M_x \xrightarrow{k_{\text{dis.ads.}}} CH_{3a} + H_a, \tag{3}$$

and

$$CH_{3a} + H_a \xrightarrow{k_{\text{ass.des.}}} CH_4 + M_x. \tag{4}$$

In Eqs. (1)–(4) M=Ni or Co, and $x=7$ or 13. In Sec. II we give details of the computations. In Sec. III the single atom results and the cluster results are discussed. In Sec. IV we summarize results and draw conclusions.

II. METHODS

We have performed quasirelativistic calculations based on density functional theory (DFT) using the Amsterdam

 0021-9606/94/101(12)/11012/9/$6.00

density functional program package (ADF) developed by Baerends *et al.*[9] The exchange-correlation potential used is based on quantum Monte Carlo simulations of Ceperley and Alder[10] of a homogeneous electron gas which has been parametrized by Vosko, Wilk, and Nusair.[11] To correct for the overbinding inherent to the local density approximation (LDA),[12] we have used a gradient corrected exchange energy functional[13] in combination with the Stoll correction[14] for correlation. For carbon a frozen core potential is used for the $1s$ electrons; for nickel and cobalt the electrons up to $3p$ are frozen. Relativistic effects were taken into account by first order perturbation theory.[15] The basis sets are of double ζ quality, with the exception of the nickel- and cobalt d-orbitals, which are triple ζ's. On all atoms polarization functions are included. As models for the substrate, we have used a single atom [Fig. 1(a)], a one layer 7-atom cluster which is extracted from a Ni(111) surface [Fig. 1(b)], and a spherical 13-atom cluster which, for reasons of symmetry, is taken from a unit cell in the hexagonally closed packed bulk [Fig. 1(c)]. For nickel clusters the bond distance was fixed at the bulk value of 2.49 Å, for cobalt clusters at the bulk value of 2.50 Å. This results in a site area per atom of 5.38×10^{-20} m^2 for nickel and 5.40×10^{-20} m^2 for cobalt, which is used for the connection between the transition state theory rate constants $k^{TST}_{ass.des.}$ and $k^{TST}_{dis.ads.}$ and their equivalents in terms of surface- and volume concentrations $k_{ass.des.}$ and $k_{dis.ads.}$.[4] The CH_3 fragment was fixed with CH distances of 1.09 Å and HCH angles of 109.48° as in CH_4. The basis for this assumption is the experimental result that the CH_3 fragment in the transition state and the dissociated state is very similar.[16]

The transition state was explicitly calculated by a four dimensional grid in the MC, MH, and CH distances and the CH_3 tilt angle with respect to the activated CH bond (θ) for the single atom models [Fig. 1(a)], and in the MC and CH distances, θ and the MMC angle (α) for the 7- and 13-atom clusters [Figs. 1(b)–1(c)]. For both the single atom systems the MH distance remains practically constant during metal atom insertion (Table II). Therefore, the MH bond distance at the 7- and 13-atom clusters was fixed at its value of the single atom system to restrict the number of degrees of freedom. The grid point energies were fitted to a second-order polynomial in the MC, MH, and CH distances and θ for the single atoms, and the MC and CH distances, θ, and α for the clusters. The obtained (fitted) energy was tested by making an additional set of calculations with the optimal geometrical parameters. The deviation between fitted and calculated energies was negligible. We included estimates of the quantum chemical tunneling phenomenon based on an unsymmetrical Eckart potential,[17] if the reaction coordinate consisted of essentially one coordinate. Vibrational calculations were performed using the conventional *GF*-method,[18] where G is the kinetic energy matrix and F the force constant matrix. Kinetic properties were calculated according to transition state theory.[19]

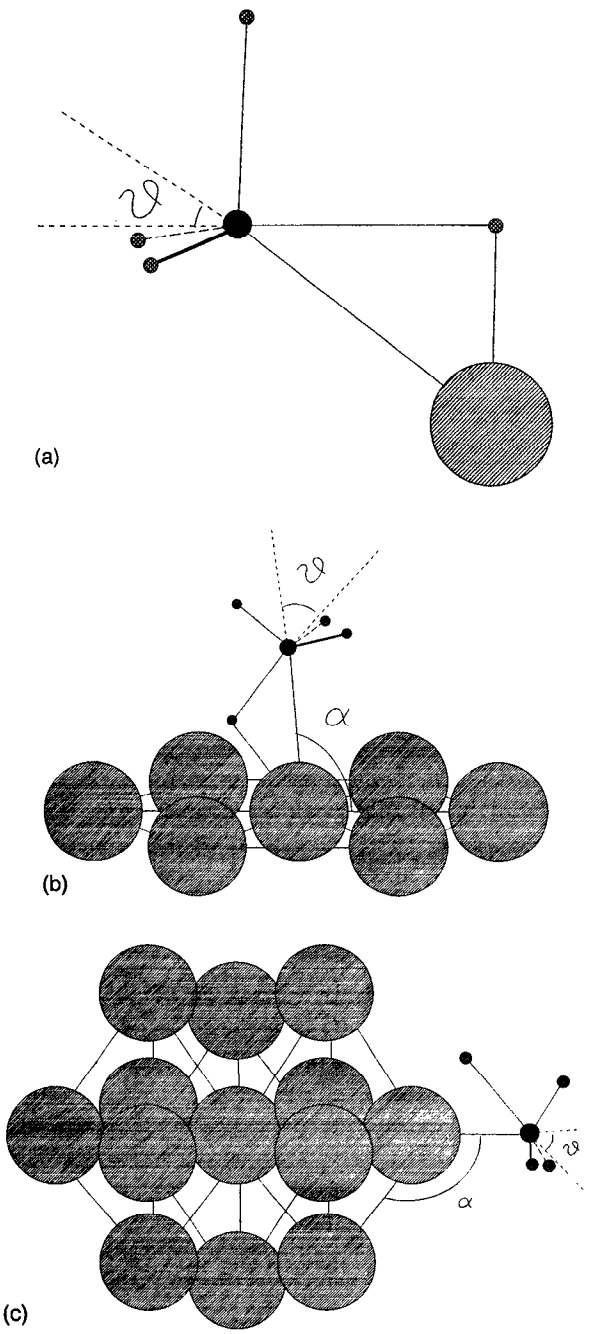

FIG. 1. Definition of optimized parameters on a single atom model (a), a one layer 7-atom cluster (b), and a spherical 13-atom cluster (c). Hydrogen atoms are denoted by diagonally cross-hatched small circles, carbon by a filled black medium circle, and metal atoms by large circles with diagonal lines. The dotted lines denote the C_{3v}-axes of the CH_3-group in the reactant- and the transition state geometry. For the single atom case, the MC bond, the MH bond, and the CH bond, which is activated by the approach of a metal atom, together with the CH_3 tilt angle with respect to the activated bond (θ) were optimized. For the polyatomic clusters, the MC bond, the activated CH bond, θ and the MMC angle (α) were optimized. For all clusters the bond distance of the bulk was used.

III. RESULTS AND DISCUSSION

A. Single atom models

Results of calculations on the atomic states of nickel and cobalt are shown in Table I. The results for nickel have been presented and discussed in earlier work,[4] but are also given here to compare with cobalt. The implementation of the program allows only for the calculation of high and low spin states of the various orbital occupations. Therefore, we can not compute separate J-states, but only J-averaged states and

TABLE I. Energies (kJ/mol) of J-averaged atomic states relative to the Ni $d^9s^1(^3D)$ state and the Co $d^7s^2(^4F+^4P)$ state.

System	J-averaged state	Experiment[a]	DFT[b]	MRCI+Q[c]	ACPF[d]	CASPT2[e]
Ni	$d^9s^1(^3D)$	0	0	0	0	0
Ni	$d^8s^2(^3F)$	3		−18		−8
Ni	$d^9s^1(^1D)$	32	17	44	29	31
Ni	$d^8s^2(^3F+^3P)$	65	67			
Ni	$d^8s^2(^1D)$	153	157			
Ni	$d^{10}(^1S)$	167	234	181		168
Co	$d^7s^2(^4F)$	−47		0		
Co	$d^8s^1(^4F)$	−7		77		
Co	$d^7s^2(^4F+^4P)$	0	0			
Co	$d^8s^1(^4F+^4P)$	34	0			
Co	$d^8s^1(^2F)$	37		108		
Co	$d^8s^1(^2F+^2P)$	76	31			
Co	$d^8s^1(a\ ^2D+b\ ^2D)$	177	93			
Co	$d^7s^2(^2G+^2P+^2H+^2G)$	192	173			
Co	$d^9(^2D)$	277	259			

[a]See Ref. 20.
[b]This work.
[c]See Ref. 21.
[d]See Ref. 22.
[e]See Ref. 23.

in the case of certain orbital occupations, linear combinations of the various terms. We conclude that in all cases DFT gives the correct order of the terms. The computed energy difference between the terms occasionally deviates significantly compared to the experimental differences,[20] but that is also the case for the MRCI+Q results.[21] The ACPF-method[22] gives only the difference between the Ni $d^9s^1(^3D)$-state and the Ni $d^9s^1(^1D)$-state, but this is accurate. The CASPT2-method[23] gives the wrong order for the most important low lying states of nickel and no data for cobalt is given.

Optimal parameters and energies of the reactant, the transition state (TS) and the dissociated state (DS) of Ni/CH_4 and Co/CH_4 are shown in Table II. We have shifted our TS and DS of cobalt with 57 kJ/mol, which is the experimental difference between the Co $d^7s^2(^4F)$-state and the Co $d^7s^2(^4P)$-state to eliminate the contribution of the excited Co $d^7s^2(^4P)$-state in our J-averaged ground state. and obtain a more realistic reactant energy. We compute a barrier for cobalt insertion of 79 kJ/mol, and an overall reaction energy of 6 kJ/mol endothermic. Blomberg *et al.*[24] computed a barrier of 101 kJ/mol using their nickel optimized geometry and the Co $d^8s^1(^2F)$ state as an asymptote. Their overall reaction energy was 42 kJ/mol endothermic. It is difficult to compare the energy barriers of cobalt, because they are given with respect to different atomic states, which can not be connected, and because Blomberg *et al.* did not optimize the TS and the DS for cobalt insertion separately. A separate optimalization for cobalt might give a lower insertion barrier. They calculated an elimination barrier of 59 kJ/mol, where we found a value of 73 kJ/mol. If we compare our separately optimized nickel- and cobalt geometries, we see that the main difference is the CH distance in both the TS and the DS, which is 0.14–0.16 Å larger in the case of cobalt. This suggests a higher barrier for cobalt insertion and a more or less the same barrier for cobalt elimination, as indeed we find.

In Table III vibrational frequencies are given for the reactant, the TS, and the DS of Ni/CH_4, Ni/CD_4, Co/CH_4, and Co/CD_4. The occurrence of one imaginary frequency in the TS region shows that we have indeed found the TS. The frequencies of the TS and the DS for cobalt are somewhat lower than those of nickel, probably due to the somewhat larger MC distance, MH distance, CH distance, and θ at these geometries. Together with the masses of the species and the rotational constants, which can be identified when

TABLE II. Geometries (Å) and energies (kJ/mol) for the Ni/CH_4 reactant, $HNiCH_3(^1A')$ TS, $HNiCH_3(^1A')$ DS, Co/CH_4 reactant, $HCoCH_3(^2A')$ TS, and $HCoCH_3(^2A')$ DS.

System	Method	R_{MC}	R_{MH}	R_{CH}	θ	E
$HNiCH_3(^1A')$ DS	DFT[a]	1.92	1.46	2.55	29.9°	−34
$HNiCH_3(^1A')$ TS	DFT	2.02	1.49	1.37	21.3°	41
Ni/CH_4[b]	DFT	∞	∞	1.08	0.0°	0
$HNiCH_3(^1A')$ DS	MRCI+Q[c]	1.98	1.47	2.55	27.0°	18
$HNiCH_3(^1A')$ TS	MRCI+Q	2.12	1.49	1.62	19.5°	83
Ni/CH_4[d]	MRCI+Q	∞	∞	1.09	0.0°	0
$HNiCH_3(^1A')$ DS	ACPF[c]	1.98	1.47	2.55	27.0°	−14
$HNiCH_3(^1A')$ TS	ACPF	2.12	1.49	1.62	19.5°	75
Ni/CH_4[d]	ACPF	∞	∞	1.09	0.0°	0
$HCoCH_3(^2A')$ DS	DFT	1.97	1.49	2.69	31.4°	6
$HCoCH_3(^2A')$ TS	DFT	2.02	1.48	1.53	26.8°	79
Co/CH_4[b]	DFT	∞	∞	1.08	0.0°	0
$HCoCH_3(^2A')$ DS	MRCI+Q	1.98	1.47	2.55	27.0°	42
$HCoCH_3(^2A')$ TS	MRCI+Q	2.12	1.49	1.62	19.5°	101
Co/CH_4[d]	MRCI+Q	∞	∞	1.09	0.0°	0

[a]This work.
[b]Ni $d^9s^1(^3D)+CH_4$ or Co $d^7s^2(^4F)+CH_4$.
[c]See Ref. 24. MRCI optimized geometries. For cobalt the nickel optimized geometries were used.
[d]Ni $d^9s^1(^1D)+CH_4$ or Co $d^7s^2(^2F)+CH_4$.

TABLE III. Vibrational frequencies, ν_i (cm^{-1}), for the Ni/CH_4 reactant, $HNiCH_3(^1A')$ TS, $HNiCH_3(^1A')$ DS, the Co/CH_4 reactant, $HCoCH_3(^2A')$ TS, $HCoCH_3(^2A')$ DS, and its deuterated analogs.

System	ν_1	ν_2	ν_3	ν_4
M/CH_4	2951	2438		
M/CD_4	2131	1929		
$HNiCH_3(^1A')$ TS	1988	1743	$682i$	607
$DNiCD_3(^1A')$ TS	1540	1258	$511i$	586
$HNiCH_3(^1A')$ DS	2238	1583	672	505
$DNiCD_3(^1A')$ DS	1605	1250	529	469
$HCoCH_3(^2A')$ TS	2290	$549i$	427	136
$DCoCD_3(^2A')$ TS	1620	$428i$	388	136
$HCoCH_3(^2A')$ DS	1544	1448	252	140
$DCoCD_3(^2A')$ DS	1104	1026	252	138

the geometries at the reactant, the TS, and the DS are determined, we can compute the rate constants for the bimolecular insertion reaction and the unimolecular elimination reaction using transition state theory according to

$$k^{\mathrm{TST}}_{\mathrm{bi.ins.}} = \frac{k_B T V}{h} \frac{(Q_v Q_r)^{\dagger}}{Q_t Q_v Q_r} e^{(-E_{\mathrm{crit}}/k_B T)} \tag{5}$$

and

$$k^{\mathrm{TST}}_{\mathrm{uni.eli.}} = \frac{k_B T}{h} \frac{(Q_v Q_r)^{\dagger}}{Q_v Q_r} e^{(-E'_{\mathrm{crit}}/k_B T)}. \tag{6}$$

In Eqs. (5) and (6) k_B denotes Boltzmann's constant, T temperature, and h Planck's constant. Q_t, Q_v, and Q_r are the translational, vibrational, and rotational partition functions for the reactant, the TS, and the DS. The translational partition function describes the relative translation of CH_4 with respect to the single atom. A dagger (†) denotes transition state partition functions. E_{crit} is the minimum energy at which reaction can occur classically (critical energy), and includes the zero point vibrational energy differences. To evaluate $k^{\mathrm{TST}}_{\mathrm{uni.eli.}}$ and $k^{\mathrm{TST}}_{\mathrm{bi.ins.}}$, we need to calculate the translational, vibrational, and rotational partition functions at the reactant, the TS, and the DS. We can restrict the number of freedom by noting the following. First, if partition functions are the same in the TS and the DS, or at the reactant and the TS, they cancel. Second, if a vibrational frequency is high ($h\nu \gg k_B T$), the partition function gives a factor of 1.0 and therefore has no contribution to the rate constant.

To find out which degrees of freedom cancel, we characterized them at the different parts of the potential energy surface. In the TS and the DS we have the following degrees of freedom: three translations of the center of mass, three overall rotations, three CH-stretches in CH_3, one methyl tilt in the mirror plane, one methyl tilt out of the mirror plane, three internal bending modes in CH_3, one internal CH_3 rotation around the C_{3v} axis, one CH-stretch, one MC-stretch and one MH-stretch. At the reactant we have the following degrees of freedom: three translations of the center of mass, three relative translations, three overall rotations of CH_4, three CH-stretches in CH_3, three internal bending modes in CH_3, one CH_3 tilt in the mirror plane, one CH_3 tilt out of the mirror plane, and one CH-stretch. By this choice of modes the partition functions of the three translations of the center of mass, the three CH-stretches of CH_3, the three internal bending modes in CH_3, and the CH_3 tilt out of the mirror plane cancel against each other. Furthermore, one internal CH_3 rotation at the TS and the DS cancels against one overall CH_4 rotation. Effectively, we have to compute at the TS and the DS the partition functions for the CH-stretch, the MC-stretch, the MH-stretch, the CH_3 tilt in the mirror plane and three overall rotations, and at the reactant three relative translations, the CH stretch, the CH_3 tilt in the mirror plane, and two overall rotations of CH_4.

Now, according to Eqs. (5) and (6) rate constants can be evaluated. The results are shown in Table IV. Γ^* denotes the ratio of quantum chemical rate to classical chemical rate as calculated by transition state theory. In the quantum chemical rate we corrected for tunneling effects by assuming that our reaction coordinate can be described by a one dimensional

TABLE IV. Unimolecular (k_1^{TST}) (s^{-1}) and bimolecular (k_2^{TST}) ($m^3\ mol^{-1}\ s^{-1}$) rate constants and their isotopic substitution ratios, classical sticking coefficients (S^{TST}), quantum sticking coefficients (S^{QM}), and ratio of quantum chemical rate to classical chemical rate (Γ^*) for different temperatures (T) (K) for Ni/CH_4, Ni/CD_4, Co/CH_4, and Co/CH_4.

System	T	$k^{\mathrm{TST}}_{\mathrm{bi.ins.}}$	k^{CH_4}/k^{CD_4}	$k^{\mathrm{TST}}_{\mathrm{uni.eli.}}$	k^{CH_4}/k^{CD_4}	S^{TST}	S^{QM}	Γ^*
Ni/CH_4	250	$2.14\times10^{+0}$		6.55×10^{-3}		1.40×10^{-08}	2.89×10^{-08}	2.064
Ni/CD_4	250	3.38×10^{-1}	6.33	3.62×10^{-3}	1.81	2.41×10^{-09}	3.56×10^{-09}	1.478
Ni/CH_4	500	$1.09\times10^{+4}$		$2.67\times10^{+5}$		5.04×10^{-05}	6.00×10^{-05}	1.190
Ni/CD_4	500	$3.63\times10^{+3}$	3.00	$1.81\times10^{+5}$	1.48	1.83×10^{-05}	2.02×10^{-05}	1.102
Ni/CH_4	750	$2.20\times10^{+5}$		$9.55\times10^{+7}$		8.29×10^{-04}	8.97×10^{-04}	1.082
Ni/CD_4	750	$9.62\times10^{+4}$	2.29	$6.83\times10^{+7}$	1.40	3.96×10^{-04}	4.14×10^{-04}	1.045
Ni/CH_4	1000	$1.10\times10^{+6}$		$1.82\times10^{+9}$		3.59×10^{-03}	3.76×10^{-03}	1.047
Ni/CD_4	1000	$5.53\times10^{+5}$	1.99	$1.34\times10^{+9}$	1.36	1.97×10^{-03}	2.02×10^{-03}	1.026
Co/CH_4	250	1.54×10^{-6}		9.54×10^{-3}		9.81×10^{-15}	1.73×10^{-14}	1.761
Co/CD_4	250	1.25×10^{-7}	12.32	6.02×10^{-3}	1.58	8.66×10^{-16}	1.14×10^{-15}	1.311
Co/CH_4	500	$1.02\times10^{+1}$		$3.06\times10^{+5}$		4.61×10^{-08}	5.15×10^{-08}	1.117
Co/CD_4	500	$2.08\times10^{+0}$	4.90	$2.33\times10^{+5}$	1.31	1.02×10^{-08}	1.09×10^{-08}	1.070
Co/CH_4	750	$2.43\times10^{+3}$		$1.06\times10^{+8}$		8.94×10^{-06}	9.40×10^{-06}	1.051
Co/CD_4	750	$6.74\times10^{+2}$	3.61	$8.23\times10^{+7}$	1.30	2.70×10^{-06}	2.78×10^{-06}	1.031
Co/CH_4	1000	$4.21\times10^{+4}$		$2.01\times10^{+9}$		1.34×10^{-04}	1.38×10^{-04}	1.029
Co/CD_4	1000	$1.36\times10^{+4}$	3.09	$1.55\times10^{+9}$	1.30	4.70×10^{-05}	4.78×10^{-05}	1.018

TABLE V. Electronic energy (E) (kJ/mol), critical energy (E_{crit}) (kJ/mol), activation energy (E_{act}) (kJ/mol), and Arrhenius pre-exponential (A) for addition ($m^3\ mol^{-1}\ s^{-1}$) and elimination (s^{-1}) for Ni/CH_4, Ni/CD_4, $CoCH_4$, and Co/CD_4.

System	Reaction	E	E_{crit}	E_{act}	A
Ni/CH_4	insertion	41	35	36	$7.62\times10^{+07}$
Ni/CD_4	insertion	41	38	39	$5.56\times10^{+07}$
Ni/CH_4	elimination	75	71	73	$1.16\times10^{+13}$
Ni/CD_4	elimination	75	72	74	$9.43\times10^{+12}$
Co/CH_4	insertion	79	64	66	$1.05\times10^{+08}$
Co/CD_4	insertion	79	67	70	$5.39\times10^{+07}$
Co/CH_4	elimination	73	70	72	$1.13\times10^{+13}$
Co/CD_4	elimination	73	71	73	$9.68\times10^{+12}$

unsymmetrical Eckart potential energy function.[17] For the boundaries of the Eckart function, we have taken the potential energy difference between the reactant and the TS and the TS and the DS, respectively, resulting in an upper bound for the tunneling correction. The justification for this one dimensional model is that analysis of our vibrational data shows that at the saddlepoint the reaction coordinate consists almost purely of the CH stretch. We can see that at low temperatures ($T=250$ K) tunneling has a pronounced effect on the reaction rate (a factor of 2.064 for Ni/CH_4 and a factor of 1.761 for Co/CH_4), and that tunneling is quite different for hydrogen and deuterium. At high temperatures ($T=1000$ K) classical rates and quantum chemical rates, which are simply obtained from Table IV by multiplication of $k^{TST}_{uni.eli.}$ or $k^{TST}_{bi.ins.}$ with Γ^*, become equal, as it should be.

Classical sticking coefficients (S^{TST}) are calculated in the following manner. We calculated the hard sphere pre-exponential (A^{HS}) by treating CH_4 and M as hard spheres,

$$A^{HS}=\pi d^2\sqrt{\frac{8k_BT}{\pi\mu_{MCH_4}}}. \tag{7}$$

In Eq. (7) πd^2 represents the hard sphere collision cross section and $\sqrt{8k_BT/\pi\mu_{MCH_4}}$ the mean speed according to the Maxwell distribution. d is given by the sum of the hard sphere radii of CH_4 and M, which are 1.91×10^{-10} m for CH_4,[25] 1.62×10^{-10} m for Ni,[26] and 1.67×10^{-10} m for Co.[26] The sticking coefficient is now simply the ratio of $k^{TST}_{bi.ins.}$ and A^{HS} and is therefore effectively the reaction probability per hard sphere collision. Analogous, the quantum sticking coefficient (S^{QM}) can be calculated as the ratio of $k^{QM}_{bi.ins.}$ and A^{HS}. The isotopic substitution ratio is almost negligible for the elimination reaction, but pronounced for the insertion reaction.

Barrier energies and Arrhenius pre-exponentials are given in Table V. The electronic energy, E, denotes the energy difference between the reactant, the TS, and the DS at the electronic potential energy surface. In the critical energy, E_{crit}, the differences in zero point energy for the reactant, the TS, and the DS have been taken into account. Using Arrhenius' rate law, we have constructed an Arrhenius plot. Figure 2(a) shows the insertion and elimination of nickel and cobalt in CH_4. The activation energy, E_{act}, is reflected in the slope, and the pre-exponential, A, in the intercept. We see that inclusion of zero point energies lowers the insertion barrier of

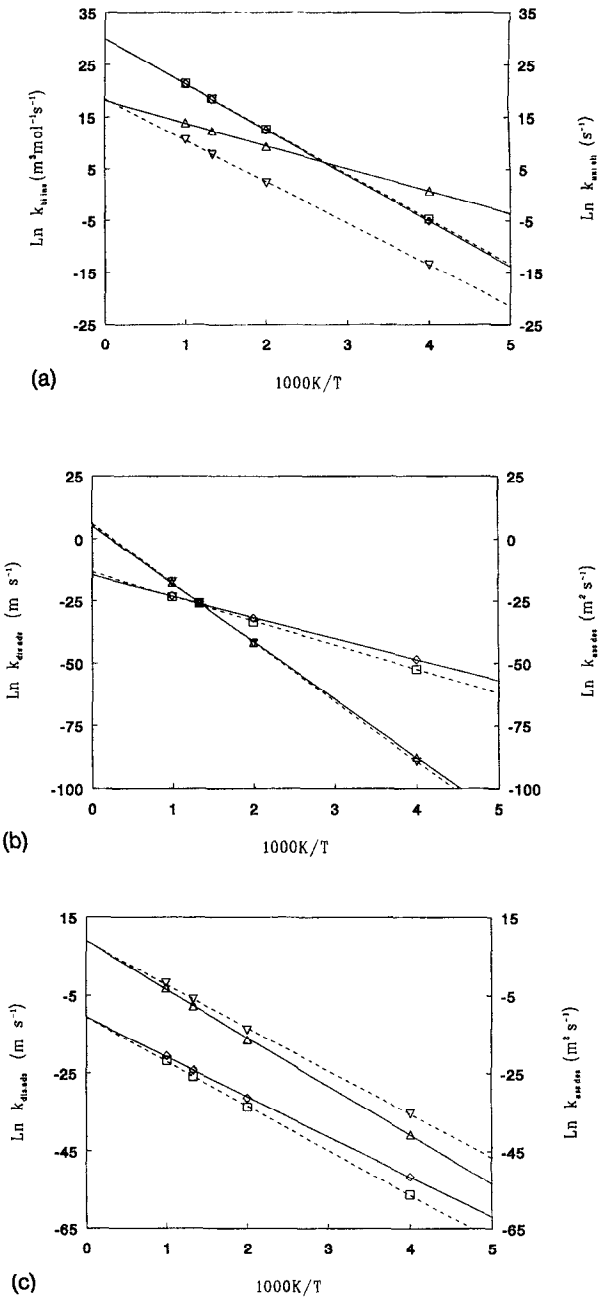

FIG. 2. Arrhenius plots for the bimolecular insertion ($k_{bi.ins.}$) and unimolecular elimination ($k_{uni.eli.}$) of Ni/CH_4 and Co/CH_4 (a), the dissociative adsorption ($k_{dis.ads.}$) and associative desorption ($k_{ass.des.}$) of Ni_7/CH_4 and Co_7/CH_4 (b), and the dissociative adsorption and associative desorption of Ni_{13}/CH_4 and Co_{13}/CH_4 (c). Solid lines for nickel, dashed lines for cobalt. The following markers are used: △, $k_{bi.ins.}$ or $k_{dis.ads.}$ nickel; ▽, $k_{bi.ins.}$ or $k_{dis.ads.}$ cobalt; ◇, $k_{uni.eli.}$ or $k_{ass.des.}$ nickel; □, $k_{uni.eli.}$ or $k_{ass.des.}$ cobalt. The intercepts show clearly that the pre-exponentials are almost the same for nickel and cobalt, but very different for an insertion- or an elimination reaction or an dissociation- or association reaction. The slopes reflect the activation energies.

Co/CH_4 by 15 kJ/mol, reflecting the relatively low frequencies at the TS and the high stretching mode frequency for CH_4. The effect of deuteration is to lower vibrational frequencies for both the TS and the Co/CH_4 reactant. Therefore,

TABLE VI. Geometries (Å) and energies (kJ/mol) of the reactant, the TS and the DS for the cluster models.

System	Method	R_{MC}	R_{MH}	R_{CH}	α	θ	E
Ni_7/CH_4 DS	DFT[a]	2.06	1.70	∞	90.0°	0.0°	142[b]
Ni_7/CH_4 TS	DFT	2.24	1.49	1.63	90.1°	26.4°	214
Ni_7/CH_4 gas	DFT	∞	∞	1.08	···	0.0°	0
Ni_{13}/CH_4 DS	DFT	1.99	1.83	∞	135.0°	0.0°	30[c]
Ni_{13}/CH_4 TS	DFT	2.07	1.49	1.80	116.8°	29.0°	121
Ni_{13}/CH_4 gas	DFT	∞	∞	1.08	···	0.0°	0
Ni_{13}/CH_4 DS	MRCI+Q[d]						
Ni_{13}/CH_4 TS	MRCI+Q	2.12	1.48	1.51	83.5°	27.0°	77
Ni_{13}/CH_4 gas	MRCI+Q	∞	∞	1.09	···	0.0°	0
Co_7/CH_4 DS	DFT	2.09	1.66	∞	90.0°	0.0°	135[e]
Co_7/CH_4 TS	DFT	2.21	1.48	1.52	88.2°	26.8°	216
Co_7/CH_4 gas	DFT	∞	∞	1.08	···	0.0°	0
Co_{13}/CH_4 DS	DFT	2.08	1.77	∞	135.0°	0.0°	8[f]
Co_{13}/CH_4 TS	DFT	2.10	1.48	1.79	119.9°	27.2°	110
Co_{13}/CH_4 gas	DFT	∞	∞	1.08	···	0.0°	0

[a]This work.
[b]Chemisorption energy H (threefold) on Ni_7; 241 kJ/mol. Chemisorption energy CH_3 (onefold) on Ni_7; 97 kJ/mol.
[c]Chemisorption energy H (threefold) on Ni_{13}; 272 kJ/mol. Chemisorption energy CH_3 (onefold) on Ni_{13}; 179 kJ/mol.
[d]Modeling a Ni(100) surface, Ref. 7.
[e]Chemisorption energy H (threefold) on Co_7; 240 kJ/mol. Chemisorption energy CH_3 (onefold) on Co_7; 105 kJ/mol.
[f]Chemisorption energy H (threefold) on Co_{13}; 270 kJ/mol. Chemisorption energy CH_3 (onefold) on Co_{13}; 202 kJ/mol.

TABLE VII. Vibrational frequencies, ν_i (cm^{-1}), of the reactant, the TS, and the DS of the cluster models.

System	ν_1	ν_2	ν_3	ν_4	ν_5	ν_6
M_x/CH_4 gas	2951	2438				
M_x/CD_4 gas	2131	1929				
Ni_7/CH_4 TS	636	499	327	152	38*i*	6
Ni_7/CD_4 TS	450	403	265	139	31*i*	5
Ni_7/CH_4 DS	1663	1014	387			
Ni_7/CD_4 DS	1319	718	353			
Ni_{13}/CH_4 TS	875*i*	636[a]	361	152[a]	31	2
Ni_{13}/CD_4 TS	633*i*	450[a]	332	139[a]	24	2
Ni_{13}/CH_4 DS	1633	1284	465			
Ni_{13}/CD_4 DS	1298	908	424			
Co_7/CH_4 TS	629	505	167	150	133*i*	5
Co_7/CD_4 TS	445	448	153	110	107*i*	4
Co_7/CH_4 DS	1056	1001	365			
Co_7/CD_4 DS	747	794	333			
Co_{13}/CH_4 TS	954*i*	629[b]	349	167[b]	35	2
Co_{13}/CD_4 TS	690*i*	445[b]	321	153[b]	27	2
Co_{13}/CH_4 DS	1947	1068	556			
Co_{13}/CD_4 DS	1544	756	507			

[a]Parallel modes of the Ni_7-cluster.
[b]Parallel modes of the Co_7-cluster.

the lowering effect on the insertion barrier is smaller (12 kJ/mol). For the elimination barrier, we see the same trends but less pronounced (3 kJ/mol for CH_4 and 2 kJ/mol for CD_4, respectively). The activation energy displays the effect on the barrier, when excited rotational and vibrational levels are populated; it is a temperature averaged barrier. The population of high vibrational frequency excited levels, e.g., CH-stretch mode at the Co/CH_4 reactant or the MH-stretch mode in the DS, will remain small at elevated temperatures, because of its high frequency and thereby associated high energy. On the contrary, the population of relatively low vibrational frequency excited levels, as those in the TS, will strongly increase, as is reflected in the vibrational partition functions and the barrier for insertion will thus increase (1–3 kJ/mol). The absolute value of the temperature averaged barrier will depend on the values of the translational, vibrational, and rotational partition functions at the reactant, the TS, and the DS.

The pre-exponential factor on going from the DS to the TS, is connected to the entropy of activation, ($\Delta S^{\ddagger}$), according to

$$A^{\mathrm{TST}} = \frac{e k_B T}{h} e^{(\Delta S^{\ddagger}/k_B T)} \tag{8}$$

and is therefore a measure for the gain or loss in entropy. At ordinary temperatures the pre-exponential in Eq. (8) is approximately 10^{13} s^{-1}. The pre-exponentials for nickel and cobalt elimination are approximately 10^{13} s^{-1}, which indicates that $\Delta S^{\ddagger}$ is approximately zero. The entropy in the TS and the DS is therefore the same. In combination with the relatively low frequencies for both the TS and the DS (see Table III), we conclude that both states are loosely bound. This can also be concluded by investigating the pre-exponential for the bimolecular insertion reaction. The pre-exponential factor on going from the reactant to the TS at ordinary temperatures for a volume of 1 m^3 is approximately 10^5 m^3 s^{-1} mol^{-1}, where we have accounted for the loss of the translational degrees of freedom by substituting for the translational partition function. Therefore, our values of 10^7–10^8 denote also a loose transition state.

B. Cluster models

Optimal parameters and adsorption energies of the Ni_7/CH_4-, Ni_{13}/CH_4-, Co_7/CH_4-, and Co_{13}/CH_4 reactant, the TS and the DS are shown in Table VI. The enormous increase in barrier height going from a single atom to a 7-atom cluster (173 kJ/mol for Ni_7, 137 kJ/mol for Co_7) has as its main cause the inclusion of the nearest neighbors of the central nickel atom at which adsorption takes place. This reduces strongly the reactivity of the central nickel atom. Although the CH bond is more stretched in the TS of Ni_{13}/CH_4 and Co_{13}/CH_4 compared to the 7-atom clusters, the barrier height for CH_4 dissociation drops by 93 kJ/mol for nickel and by 106 kJ/mol for cobalt. This is due to two effects. First, the metal atom at which adsorption takes place has now five nearest neighbors, two next-nearest neighbors, and four next-next-nearest neighbors as holds for all surface atoms in this substrate model. In this respect it is a better model for any infinite surface plane than the 7-atom cluster. Also the average strength of the metal–metal bonds is now strongly moderated, as can be concluded by dividing the formation energy of the cluster through the number of bonds formed. In Ni_7 this average bond strength is 152 kJ/mol, in Ni_{13} 106 kJ/mol, whereas in bulk nickel the average bond strength is 71 kJ/mol according to Kittel.[27] For Co_7 we find a value of 102 kJ/mol, for Co_{13} a value of 80 kJ/mol and for bulk cobalt a value of 70 kJ/mol is given.[27] A surface atom of the 13-atom cluster can therefore form more easily a bond

TABLE VIII. Rate constant for dissociative adsorption ($k_{\text{dis.ads.}}$) (m s^{-1}) and isotopic substitution ratio, rate constant for associative desorption ($k_{\text{ass.des.}}$) ($\text{m}^2\,\text{s}^{-1}$), and isotopic substitution ratio, classical sticking coefficients (S^{TST}), quantum sticking coefficients (S^{QM}), and ratio of quantum chemical rate to classical chemical rate (Γ^*) for the cluster models.

System	T	$k_{\text{dis.ads.}}$	$k^{\text{CH}_4}/k^{\text{CD}_4}$	$k_{\text{ass.des.}}$	$k^{\text{CH}_4}/k^{\text{CD}_4}$	S^{TST}	S^{QM}	Γ^*
Ni_7/CH_4	250	9.22×10^{-39}		9.17×10^{-22}		6.42×10^{-41}		
Ni_7/CD_4	250	3.05×10^{-40}	30.27	2.23×10^{-22}	4.11	2.37×10^{-42}		
Ni_7/CH_4	500	8.74×10^{-19}		1.61×10^{-14}		4.30×10^{-21}		
Ni_7/CD_4	500	1.45×10^{-19}	6.03	6.93×10^{-15}	2.32	7.98×10^{-22}		
Ni_7/CH_4	750	6.56×10^{-12}		5.82×10^{-12}		2.64×10^{-14}		
Ni_7/CD_4	750	1.89×10^{-12}	3.47	2.97×10^{-12}	1.96	8.51×10^{-15}		
Ni_7/CH_4	1000	2.31×10^{-08}		1.27×10^{-10}		8.03×10^{-11}		
Ni_7/CD_4	1000	8.62×10^{-09}	2.68	6.96×10^{-11}	1.82	3.36×10^{-11}		
Ni_{13}/CH_4	250	2.05×10^{-18}		4.17×10^{-23}		1.43×10^{-20}	5.50×10^{-20}	3.862
Ni_{13}/CD_4	250	5.14×10^{-20}	39.80	6.27×10^{-24}	6.65	4.00×10^{-22}	7.48×10^{-22}	1.870
Ni_{13}/CH_4	500	8.08×10^{-08}		2.35×10^{-14}		3.98×10^{-10}	5.29×10^{-10}	1.330
Ni_{13}/CD_4	500	1.12×10^{-08}	7.21	7.86×10^{-15}	3.00	6.17×10^{-11}	7.14×10^{-11}	1.158
Ni_{13}/CH_4	750	4.67×10^{-04}		2.88×10^{-11}		1.88×10^{-06}	2.13×10^{-06}	1.134
Ni_{13}/CD_4	750	1.15×10^{-04}	4.07	1.21×10^{-11}	2.39	5.16×10^{-07}	5.51×10^{-07}	1.068
Ni_{13}/CH_4	1000	4.58×10^{-02}		1.18×10^{-09}		1.59×10^{-04}	1.24×10^{-04}	1.074
Ni_{13}/CD_4	1000	1.47×10^{-02}	3.12	5.42×10^{-10}	2.18	5.72×10^{-05}	5.94×10^{-05}	1.038
Co_7/CH_4	250	1.94×10^{-39}		1.76×10^{-23}		1.35×10^{-41}		
Co_7/CD_4	250	5.73×10^{-41}	33.86	5.50×10^{-24}	3.20	4.46×10^{-43}		
Co_7/CH_4	500	6.37×10^{-19}		3.31×10^{-15}		3.13×10^{-21}		
Co_7/CD_4	500	1.00×10^{-19}	6.37	1.58×10^{-15}	2.09	5.51×10^{-22}		
Co_7/CH_4	750	7.31×10^{-12}		5.82×10^{-12}		2.94×10^{-14}		
Co_7/CD_4	750	2.02×10^{-12}	3.62	2.97×10^{-12}	1.96	9.09×10^{-15}		
Co_7/CH_4	1000	3.19×10^{-08}		7.95×10^{-11}		1.11×10^{-10}		
Co_7/CD_4	1000	1.15×10^{-08}	2.78	4.40×10^{-11}	1.81	4.47×10^{-11}		
Co_{13}/CH_4	250	4.27×10^{-16}		3.90×10^{-25}		2.97×10^{-18}	1.63×10^{-17}	5.476
Co_{13}/CD_4	250	1.05×10^{-17}	40.60	5.56×10^{-26}	7.02	8.19×10^{-20}	1.75×10^{-19}	2.141
Co_{13}/CH_4	500	1.07×10^{-06}		2.20×10^{-15}		5.29×10^{-09}	7.44×10^{-09}	1.407
Co_{13}/CD_4	500	1.47×10^{-07}	7.32	7.04×10^{-16}	3.13	8.08×10^{-10}	9.62×10^{-10}	1.191
Co_{13}/CH_4	750	2.48×10^{-03}		5.83×10^{-12}		9.97×10^{-06}	1.16×10^{-05}	1.162
Co_{13}/CD_4	750	6.01×10^{-04}	4.13	2.36×10^{-12}	2.47	2.70×10^{-06}	2.92×10^{-06}	1.081
Co_{13}/CH_4	1000	1.54×10^{-01}		3.52×10^{-10}		5.36×10^{-04}	5.84×10^{-04}	1.089
Co_{13}/CD_4	1000	4.87×10^{-02}	3.16	1.57×10^{-10}	2.28	1.90×10^{-04}	1.98×10^{-04}	1.045

with an adsorbate than the 7-atom cluster. Secondly, the steric repulsion between the hydrogen atom of the activated CH bond and the surface is far less for the 13-atom cluster, because the surface plane is now more parallel with the dissociating bond [see Figs. 1(b)–1(c)]. The barrier for associative desorption raises for both nickel and cobalt with 20 kJ/mol relative to the 7-atom clusters.

Analogous to the single atom models we can use transition state theory to compute rate constants. The formula for dissociative adsorption is given by

$$k^{\text{TST}}_{\text{dis.ads.}} = \frac{k_B T}{h} \frac{Q^{\dagger}_v}{Q_t Q_v Q_r} e^{(-E_{\text{crit}}/k_B T)} \tag{9}$$

and for associative desorption by

$$k^{\text{TST}}_{\text{ass.des.}} = \frac{k_B T}{h} \frac{Q^{\dagger}_v}{Q_t Q_v} e^{(-E'_{\text{crit}}/k_B T)}. \tag{10}$$

The translational partition function describes now the relative translation of CH_4 with respect to the substrate or, on the substrate, the two absolute and relative translations of CH_3 and H thus implying a mobile DS. The connection between $k^{\text{TST}}_{\text{dis.ads.}}$ and $k_{\text{dis.ads.}}$ and between $k^{\text{TST}}_{\text{ass.des.}}$ and $k_{\text{ass.des.}}$ is discussed in earlier work.[4] To evaluate $k^{\text{TST}}_{\text{dis.ads.}}$ and $k^{\text{TST}}_{\text{ass.des.}}$, we need to calculate the translational, vibrational, and rotational partition functions for the reactant, the TS and the DS.

To find out which degrees of freedom cancel, we characterized them at the different geometries bearing in mind that our cluster represents an (infinite) surface of infinite mass. Therefore overall translations and rotations of the cluster are irrelevant and internal lattice vibrations (phonons) are neglected. With these premisses we have determined the degrees of freedom at the TS. Three modes determine the absolute position of hydrogen; one MH stretch, one CH stretch, and one translation of hydrogen perpendicular to the mirror plane. Three modes determine the absolute position of the methyl group; one MC stretch, one MMC angle (α), and one translation of CH_3 perpendicular to the mirror plane. Three modes determine the orientation of the methyl group; the CH_3 tilt angle in the mirror plane (θ), one methyl tilt out of the mirror plane, and one internal CH_3 rotation around the internal C_{3v} axis. Finally, there are six internal CH_3 modes; three CH stretches and three internal bending modes adding up to a total of 15 degrees of freedom. For the reactant we have nine internal (vibrational) modes of CH_4, four of which are CH stretches, three are CH_3 internal bending modes, and two are wagging modes, one in the mirror plane and one out

TABLE IX. Electronic energy (E) (kJ/mol), critical energy (E_{crit}) (kJ/mol), activation energy (E_{act}) (kJ/mol), and Arrhenius pre-exponential (A^{plot}) for dissociative adsorption ($m\,s^{-1}$) and associative desorption ($m^2\,s^{-1}$) for the cluster models.

System	Reaction	E	E_{crit}	E_{act}	A^{plot}
Ni_7/CH_4	dissociative adsorption	214	188	194	$2.11\times10^{+02}$
Ni_7/CD_4	dissociative adsorption	214	194	200	$1.77\times10^{+02}$
Ni_7/CH_4	associative desorption	72	66	71	5.15×10^{-07}
Ni_7/CD_4	associative desorption	72	68	73	3.77×10^{-07}
Ni_{13}/CH_4	dissociative adsorption	121	96	104	$8.53\times10^{+03}$
Ni_{13}/CD_4	dissociative adsorption	121	103	111	$6.47\times10^{+03}$
Ni_{13}/CH_4	associative desorption	91	78	86	2.70×10^{-05}
Ni_{13}/CD_4	associative desorption	91	81	89	1.86×10^{-05}
Co_7/CH_4	dissociative adsorption	216	193	199	$5.41\times10^{+02}$
Co_7/CH_4	dissociative adsorption	216	199	206	$4.53\times10^{+02}$
Co_7/CH_4	associative desorption	81	75	81	5.58×10^{-05}
Co_7/CH_4	associative desorption	81	77	83	4.62×10^{-05}
Co_{13}/CH_4	dissociative adsorption	110	85	92	$7.24\times10^{+03}$
Co_{13}/CD_4	dissociative adsorption	110	91	99	$5.43\times10^{+03}$
Co_{13}/CH_4	associative desorption	102	88	95	2.53×10^{-05}
Co_{13}/CD_4	associative desorption	102	91	98	1.72×10^{-05}

of the mirror plane. Together with three rotations of CH_4 and three relative translations of CH_4 with respect to the surface, they make up 15 independent degrees of freedom. For the DS we have six internal CH_3 modes of which three are CH stretches, and three internal bending modes. Three modes determine the relative CH_3 position; two CH_3 wagging modes (θ, and one wagging mode out of the mirror plane), and one internal CH_3 rotation around the internal C_{3v} axis. One mode determines the absolute position of CH_3 perpendicular to the surface; the MC stretch. Two (vibrational) modes determine the absolute position of CH_3 parallel to the surface, which are two translations in the mobile model. Analogously for hydrogen, one mode determines the absolute position of hydrogen perpendicular to the surface; the MH stretch. Two modes determine the absolute position of hydrogen parallel to the surface, which are again two translations in the mobile model. Together, these modes add up again to a total of 15 degrees of freedom.

The six internal CH_3 modes cancel at all geometries. Also, one CH_3 rotation around the C_{3v}-axis at the TS and the DS cancels against one overall CH_4 rotation. Finally, the CH_3 wagging mode out of the mirror plane cancels at the reactant, the TS and the DS. Therefore, only the following modes need explicit computation. For the reactant three relative translations of CH_4 with respect to the surface, two overall rotations of CH_4, θ, and the CH stretch. At the TS α, θ, the CH stretch, the MC stretch, the MH stretch, the CH_3 translation perpendicular to the mirror plane and the H translation perpendicular to the mirror plane. At the DS θ, the MC stretch, the MH stretch, and the four translations parallel to the surface. We have not explicitly calculated the MH stretch mode, because in the G-matrix only the hydrogen mass is involved, which will result in a high frequency. As a consequence, the corresponding vibrational partition function will be 1.0. The frequencies are displayed in Table VII for both CH_4 and CD_4 on the 7- and 13-atom clusters of nickel and cobalt. For the 7-atom clusters the imaginary frequency at the TS is a mixture of all modes. On the 13-atom clusters it consists almost purely of the CH stretch and in this case we can again estimate the quantum chemical tunneling effect on the reaction rate.

The rate constants are calculated according to Eqs. (9) and (10). The results are shown in Table VIII for CH_4 and CD_4 at different temperatures. The CH_4 sticking coefficient is now given by the ratio of $k_{dis.ads.}$ and A^{HS}, which is now

$$A^{HS}=\sqrt{\frac{k_BT}{2\pi m_{CH_4}}}. \tag{11}$$

The isotopic substitution ratio is significant for dissociative adsorption, especially at low temperatures. The high imaginary frequency of the 13-atom clusters is reflected in the large values of Γ^* at $T=250$ K. Tunneling is easier through a sharply peaked barrier, which is associated with a high imaginary frequency. The sticking coefficients are clearly too low for the 7-atom cluster as a result of the very high dissociation barrier. This defect is remedied when we use the 13-atom cluster as a substrate model. Beebe *et al.*[28] find an activation energy of 53 kJ/mol for CH_4 on Ni(111) and sticking coefficients of 10^{-8}–10^{-7} at $T=500$ K. Geerlings *et al.*[29] report a CH_4 dissociation barrier on Co(0001) of 70 kJ/mol. Our sticking coefficients on Ni_{13} at $T=500$ K are of the order 10^{-10}, which is somewhat too small, and our dissociation barrier without kinetical corrections is 121 kJ/mol, which is somewhat too high. The effect of zero point vibrational energy and temperature on barrier heights is shown in Table IX and is qualitatively the same as for our single atom models. Arrhenius plots for CH_4 dissociation and CH_3/H association on Ni_7/Co_7 and Ni_{13}/Co_{13} are shown in Figs. 2(b)–2(c), respectively. According to our calculations, the barrier for CH_4 dissociation is the same on Ni_7 and Co_7, but somewhat lower on Co_{13} compared to Ni_{13}. Desorption is easier on nickel for both cluster models. Zaera[30] reports a desorption barrier of 71 kJ/mol on nickel, which is in good agreement with our calculated barrier on Ni_7 (72 kJ/mol) and Ni_{13} (91 kJ/mol).

If the entropy of activation ($\Delta S^{\ddagger}$) equals zero, the pre-exponential factor is approximately 10^2 m s^{-1} for an adsorption reaction and 10^{-6} $m^2\,s^{-1}$ for a bimolecular desorption reaction.[19] The pre-exponentials for adsorption denote therefore that there is essentially no entropy of activation. This can be understood by realizing that although three relative translations are lost going from the reactant to the TS, the vibrations at TS are very loose modes and the activated CH_4 can rotate freely on the surface. For the desorption reaction some entropy is lost. Four translation modes are lost in going from the DS to the TS, but this is once again counteracted by the very loose vibrations in the TS, thus limiting the overall effect.

IV. CONCLUSIONS

We have computed the J-averaged atomic energy levels of nickel and cobalt. The order of the levels is produced correctly. Subsequently, we have determined the TS and the DS of reactions (1)–(4). In addition, we calculated rotational constants and vibrational frequencies and used transition state theory to calculate rate constants and sticking coeffi-

cients. The barrier for insertion of a nickel atom turns out to be 41 kJ/mol, the barrier for cobalt insertion 79 kJ/mol. For nickel elimination we find a barrier of 75 kJ/mol and for cobalt elimination of 73 kJ/mol. The higher insertion barrier of cobalt and the almost equal barrier for elimination is due to the looser structure of the TS and the DS of cobalt. This is also reflected in the vibrational frequencies.

On the 7-atom clusters the CH_4 dissociation barriers are too high and almost the same for nickel and cobalt. The CH_3/H association barrier is 7 kJ/mol lower on Ni_7 and the value of 72 kJ/mol for nickel compares very well with the reported value of Zaera[30] of 71 kJ/mol. On the 13-atom clusters the CH_4 dissociation barrier drops sharply to 121 kJ/mol for nickel and 110 kJ/mol for cobalt. The association barriers are now 91 kJ/mol on nickel and 102 kJ/mol on cobalt. Also the endothermicity now drops to 30 kJ/mol for nickel and 8 kJ/mol on cobalt. Vibrational modes are very loose on both clusters. Calculated sticking coefficients on the Ni_{13}-cluster at $T=500$ K are two orders of magnitude away from the experimental ones. This is due to the computed barrier height (121 kJ/mol), which is still significantly higher than the experimental value (53 kJ/mol). We also made an estimate of hydrogen and deuterium tunneling effects, which turned out to be small, except at low temperatures for the 13-atom clusters.

ACKNOWLEDGMENTS

All calculations were performed with the ADF program on the Cray Y-MP4/464 at SARA, Amsterdam. This work has been supported by the Netherlands Foundation for Chemical Research (SON) with financial aid from the Netherlands Organization of Pure and Scientific Research (NWO). The computer time on the Cray Y-MP4/464 was subsidized by the Foundation for the use of supercomputers, National Computing Facilities (NCF).

[1] J. P. Van Hook, Catal. Rev. Sci. Eng. **21**, 1 (1980).
[2] F. Fischer and H. Tropsch, Brennst. Chem. **7**, 97 (1926); F. Fischer and H. Tropsch, Chem. Ber. **59**, 830 (1926).
[3] J. R. Rostrup-Nielsen, *Catalysis- Science and Technology*, edited by J. R. Anderson and M. Boudart (Springer, Berlin, 1984).
[4] H. Burghgraef, A. P. J. Jansen, and R. A. van Santen, J. Chem. Phys. **98**, 8810 (1993); H. Burghgraef, A. P. J. Jansen, and R. A. van Santen, Chem. Phys. **177**, 407 (1993).
[5] J. T. Yates, Jr., S. M. Gates, and J. N. Russell, Jr., Surf. Sci. **164**, L839 (1985).
[6] R. C. Brady III and R. Pettit, J. Am. Chem. Soc. **102**, 6181 (1980); R. C. Brady III and R. Pettit, J. Am. Chem. Soc. **103**, 1287 (1981).
[7] H. Yang and J. L. Whitten, J. Chem. Phys. **96**, 5529 (1992); O. Swang, K. Faegri, Jr., O. Gropen, U. Wahlgren, and P. E. M. Siegbahn, Chem. Phys. **156**, 379 (1991).
[8] A. C. Luntz and J. Harris, Surf. Sci. **258**, 397 (1991); A. C. Luntz and J. Harris, J. Vac. Sci. Technol. A **10**, 2292 (1992).
[9] Amsterdam density-functional (ADF) program developed by Baerends and co-workers; E. J. Baerends, D. E. Ellis, and P. Ros, Chem. Phys. **2**, 41 (1988); P. M. Boerrigter, G. te Velde and E. J. Baerends, Int. J. Quantum Chem. **33**, 87 (1988); G. te Velde and E. J. Baerends, J. Comput. Phys. **99**, 84 (1992); D. Post and E. J. Baerends, J. Chem. Phys. **78**, 5663 (1983); E. J. Baerends and A. Rozendaal, *Quantum Chemistry: The Challenge of Transition Metals and Coordination Chemistry*, edited by A. Veillard (Reidel, Dordrecht, 1986); P. J. van den Hoek, A. W. Kleyn, and E. J. Baerends, Comments Atom. Mol. Phys. **23**, 93 (1989).
[10] D. M. Ceperley and B. J. Alder, Phys. Rev. Lett. **45**, 566 (1980).
[11] S. H. Vosko, L. Wilk, and M. Nusair, Can. J. Phys. **58**, 1200 (1980); J. P. Perdew and A. Zunger, Phys. Rev. B **23**, 5048 (1981).
[12] A. D. Becke, Int. J. Quantum Chem. **27**, 585 (1985).
[13] A. D. Becke, Phys. Rev. A **38**, 3098 (1988).
[14] H. Stoll, C. M. E. Pavlidou, and H. Preuss, Theor. Chim. Acta **49**, 143 (1978); H. Stoll, E. Golka, and H. Preuss, Theor. Chim. Acta **55**, 29 (1980).
[15] J. G. Snijders and E. J. Baerends, Mol. Phys. **36**, 1789 (1978); J. G. Snijders, E. J. Baerends, and P. Ros, *ibid.* **38**, 1909 (1979).
[16] M. B. Lee, Q. Y. Yang, and S. T. Ceyer, J. Chem. Phys. **87**, 2724 (1987).
[17] H. S. Johnston and J. Heicklen, J. Phys. Chem. **66**, 532 (1962); H. S. Johnston and D. Rapp, J. Am. Chem. Soc. **83**, 1 (1961).
[18] E. B. Wilson, J. C. Decius, and P. C. Cross, *Molecular Vibrations. Theory of Infrared and Raman Vibrational Spectra* (McGraw–Hill, New York, 1955).
[19] R. G. Gilbert and S. C. Smith, *Theory of unimolecular and recombination reactions* (Blackwell, Oxford, 1990); M. Boudart and G. Djéga-Mariadassou, *Kinetics of Heterogeneous Catalytic Reactions* (Princeton University, Princeton, 1984).
[20] C. E. Moore, *Atomic Energy Levels* (National Bureau of Standards, Washington D.C., 1952).
[21] C. W. Bauschlicher, P. E. M. Siegbahn, and L. G. M. Petterson, Theor. Chim. Acta **74**, 479 (1988); P. E. M. Siegbahn, M. R. A. Blomberg, and C. W. Bauschlicher, J. Chem. Phys. **81**, 1373 (1984).
[22] M. R. Blomberg, P. E. M. Siegbahn, and M. Svensson, J. Phys. Chem. **95**, 4313 (1991).
[23] K. Andersson and B. O. Roos, Chem. Phys. Lett. **191**, 507 (1992).
[24] M. R. Blomberg, P. E. M. Siegbahn, U. Nagashima and J. Wennerberg, J. Am. Chem. Soc. **113**, 424 (1991).
[25] G. W. C. Kaye and T. H. Laby, *Tables of Physical and Chemical Constants* (Longmans, London, 1957).
[26] C. F. Fischer, *The Hartree Fock Method for Atoms* (Wiley, New York, 1954).
[27] C. Kittel, *Introduction to Solid State Physics* (Wiley, New York, 1953).
[28] T. P. Beebe, D. W. Goodman, B. D. Kay, and J. T. Yates, J. Chem. Phys. **87**, 2305 (1987).
[29] J. C. C. Geerlings, M. C. Zonnevylle, and C. P. M. de Groot, Surf. Sci. **241**, 302 (1991).
[30] F. Zaera, Surf. Sci. **262**, 335 (1992).